Nonequilibrium transport and electron-glass effects in thin Ge_xTe films

Z. Ovadyahu
Racah Institute of Physics, The Hebrew University, Jerusalem 91904, Israel
(Received 7 August 2016; published 28 October 2016)

We report on results of nonequilibrium transport measurements made on thin films of germanium-telluride (Ge_xTe) at cryogenic temperatures. Owing to a rather large deviation from stoichiometry (≈10% of Ge vacancies), these films exhibit *p*-type conductivity with carrier concentration $N \geqslant 10^{20}$ cm^{-3} and can be made either in the diffusive or strongly localized regime by a judicious choice of preparation and post-treatment conditions. In both regimes, the system shows persistent photoconductivity following excitation by a brief exposure to infrared radiation. Persistent photoconductivity is also observed in Ge_xTe samples alloyed with Mn. However, in both Ge_xTe and $GeMn_xTe_y$, the effect is much weaker than that observable in $GeSb_xTe_y$ alloys, suggesting that antimony plays an important role in the phenomenon. Structural studies of these films reveal an unusual degree of texture that is rarely realized in strongly disordered systems with high carrier concentrations. Anderson-localized samples of Ge_xTe exhibit nonergodic transport which is characteristic of intrinsic electron glasses, including a well-developed memory dip and slow relaxation of the excess conductance created in the excited state. These results support the conjecture that electron-glass effects with inherently long relaxation times is a generic property of all Anderson-localized systems with large carrier concentration.

DOI: 10.1103/PhysRevB.94.155151

I. INTRODUCTION

The noninteracting Anderson-insulating phase has been called a Fermi glass [1], presumably inspired by the spatial arrangement of the localized electronic wave functions resembling an amorphous structure. Further considerations, admitting for the long-range Coulomb interaction inevitably present in a medium devoid of metallic screening, led several authors to suggest that a glassy phase, so-called electron glass (EG), should be observable in real systems [2–11].

Experimental observations consistent with the anticipated glassy behavior were reported in several Anderson-localized systems [12,13]. On the other hand, these effects were not seen in either Si or GaAs systems that are readily made insulating and exhibit strong-localization transport properties. To some researchers, this shed doubt on the notion that the electron glass is a generic phenomenon peculiar to the Anderson-insulating regime.

It has been conjectured that the absence of electron-glass features in Si and GaAs is related to their relative low carrier concentration N [14]. This was based on the observation that the dynamics in amorphous indium-oxide films [15] becomes much faster once $N \leqslant 10^{20}$ cm^{-3}. To date, a common feature in *all* Anderson insulators that exhibit intrinsic EG effects, *in addition* to being strongly localized, is their high carrier concentrations, typically with $N \geqslant 10^{20}$ cm^{-3}. By "intrinsic" we mean that the nonergodic effects appear in a given substance *independently* of the way the sample was prepared to achieve the required parameters (resistance at the measuring temperature, carrier concentration, and dimensionality determined by the hopping length to thickness ratio). Most importantly, the system has to exhibit a memory dip with a width that is commensurate with the carrier concentration of the material [14]. This distinction is important: slow conductance relaxation by itself is not necessarily a sign for EG, and slow relaxation (and $1/f$ noise) may occur in lightly doped semiconductors, presumably due to extrinsic effects [13].

The correlation between high carrier concentration and sluggish relaxation rates may suggest the relevance of many-body effects. However, a case may also be made for the difference in *disorder* being the reason behind the correlation with carrier concentration. Note that the requirement of strong localization means that a system with higher carrier concentration has perforce more *disorder* (required to overcome the higher kinetic energy associated with higher carrier concentration). One may then argue that the reason for the slow relaxation (and the various glassy features) exhibited by systems with higher Fermi energies is their considerably larger disorder rather than due to correlation effects. It may transpire that there is a peculiar *type* of disorder that exists in the high-n systems that lightly doped semiconductors cannot sustain, and it is this "defect" which slows down the relaxation of the system from an out-of-equilibrium state. It is therefore of interest to experimentally test more systems with diversified structural properties.

This work describes transport measurements on Ge_xTe samples, yet another system with carrier concentration [16] $N \geqslant 10^{20}$ cm^{-3}, somewhat above the empirical limit for observing electron-glass effects (when the system is strongly localized). Comparison with films made with the alloy $GeSb_xTe_y$ reveals a *much* weaker persistent photoconductivity [17] (PPC) in the Ge_xTe films. The relaxation law from the photoexcited state also differs from that observed in $GeSb_xTe_y$ presumably associated with another kind of a defect. The microstructure of the Ge_xTe films prepared by the method of this work shows some uncommon features, such as preferred orientation (texture) over an extremely large spatial scale, which is a single-crystal-like attribute. Yet, Anderson-localized films of this material exhibit nonequilibrium transport effects, including a memory dip characteristic of the electron-glass phase just like that found in all previously studied systems. The implications of these findings for the origin of slow relaxation of electron glasses are discussed.

A. Sample preparation and characterization

Samples used in this work were prepared by e-gun depositing GeTe onto room-temperature substrates in a

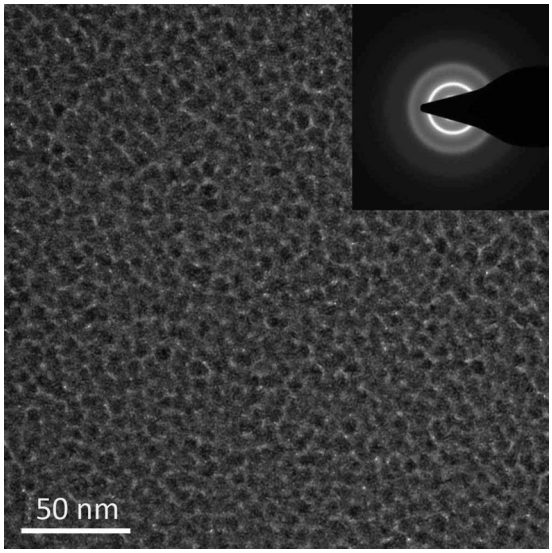

FIG. 1. Bright-field micrograph and associated diffraction pattern of the as-deposited Ge_xTe film. The lumpy appearance of the film morphology is characteristic of many amorphous structures and includes the contribution of the amorphous carbon that is the substrate in this case.

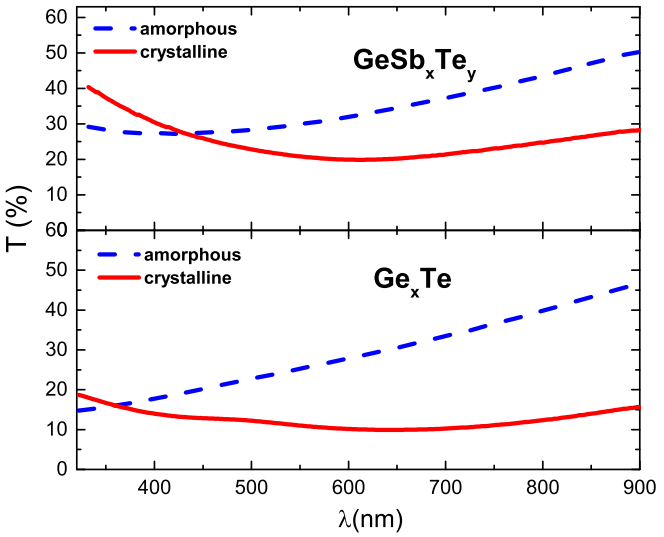

FIG. 2. Optical transmission through a 50 Å Ge_xTe film deposited on a 1 mm glass slide compared with that of a 120 Å $GeSb_xTe_y$ film [13].

high-vacuum system (base pressure 1×10^{-7} mbar) using rates of 1–2 Å/sec. The source material was 99.999% pure GeTe (Equipment Support Company). Film thickness was in the range of 30–75 Å. Lateral dimensions of the samples used for the low-temperature studies were 0.3–0.5 mm long and 0.5 mm wide. Two types of substrates were used: 1-mm-thick microscope glass slides and a 0.5 μm SiO_2 layer thermally grown on ⟨100⟩ silicon wafers. These were boron doped and had bulk resistivity $\rho \simeq 2 \times 10^{-3}$ Ω cm, deep into the degenerate regime. This makes this substrate suitable to perform as a gate electrode even at low temperatures. Samples deposited on these wafers were configured as three-terminal devices for field-effect measurements. These were designed to probe $\partial n/\partial \mu(E)$, the thermodynamic density of states versus energy of the material, as well as to test for electron-glass behavior. Samples prepared on microscope glass slides were mainly used for optical characterization and for Hall-effect measurements, both performed at room temperature.

Each deposition batch included samples for optical excitation measurements, for Hall-effect measurements, and for structural and chemical analysis using a transmission electron microscope (TEM). For the latter study, carbon-coated Cu grids were put close to the sample during its deposition and received the same post-treatment as the samples used for transport measurements.

The Philips Tecnai F20 G2 was used to characterize the films' composition [using energy dispersive spectroscopy (EDS)] and microstructure. The EDS typically showed Ge deficiency, so we refer to our deposited films as Ge_xTe. The Cary-1 spectrophotometer was used for optical measurements.

Films deposited at room temperature were amorphous. TEM and the associated diffraction pattern of a typical Ge_xTe sample deposited an hour prior to being inserted into the TEM are shown in Fig. 1. Crystalline samples of Ge_xTe were obtained from the amorphous Ge_xTe deposits by subjecting them to temperatures in the range of 470–490 K for 2–3 minutes. The amorphous-crystalline transformation is reflected in the optical properties of the films as a mild change in color tint. In this regard, the result is very similar to the corresponding situation in the $GeSb_xTe_y$ compound studied previously [12], as can be seen in the comparison shown in Fig. 2.

In terms of other properties, however, there are significant differences between our crystalline versions of Ge_xTe and the $GeSb_xTe_y$. In particular, their microstructure is different: while both systems exhibit mosaic film structure with a tight, space-filling packing of the crystallites, the Ge_xTe film shows a much more pronounced preferred orientation extending over large scales. This may be seen in both transmission electron microscope (TEM) micrographs depicted in Fig. 3 (same sample as shown in Fig. 1 after crystallization at 485 K) and Fig. 4 (same sample after being "aged" for a week). The diffraction patterns in these figures were taken in a selected-area mode covering 0.8 micron circle diameter. Pronounced preferred orientation was still conspicuous using a selected area of 4 microns, which is at least one order of magnitude larger than the average size of the grains in the studied films. This extensive texture, extending over a scale much larger than a typical grain size, was uniformly observed across the 3 mm TEM grid by scanning it with a constant electron beam.

We found it hard to get films with appreciable sheet resistance even in a quite thin specimen. The reason for that is presumably the reduced grain-boundary scattering and better mobility relative to that observed in the $GeSb_xTe_y$ alloys (assuming that impurity contents and carrier concentration are the same). Special measures had to be taken in fabricating films with high values for $R_\square$ (which were required for observing electron-glass properties). These included reducing the film thickness (down to 30 Å relative to the constant 120 Å used in the study of $GeSb_xTe_y$ [13]) and aging the films

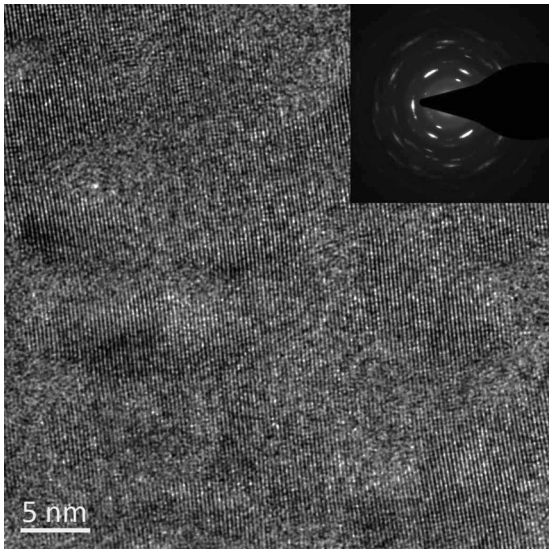

FIG. 3. Bright-field micrograph and associated diffraction pattern of the sample in Fig. 1 after crystallization. The extensive texture is clearly observed in both the image and the diffraction pattern despite the plethora of point defects. The diffraction pattern is consistent with the rhombohedral (R-3m) phase of GeTe.

in the laboratory atmosphere. A micrograph and associated diffraction of an aged film are shown in Fig. 4.

The room-temperature resistance of our films spans the range 600 Ω–29 kΩ, which yielded 0.8 kΩ–5.6 MΩ at $T \approx 4$ K. The upper limit of this range was obtained by reducing the film thickness to 30 Å and exposing the sample to the laboratory atmosphere for several days. However, we were yet unable to produce films with $R_\square > 5.6$ MΩ at 4.1 K. By comparison, using the $GeSb_xTe_y$ alloy, it was rather easy to obtain samples with $R_\square$ as high as 50 MΩ, even with films that were: 3–4 nm, thicker [12] than the Ge_xTe used in this work.

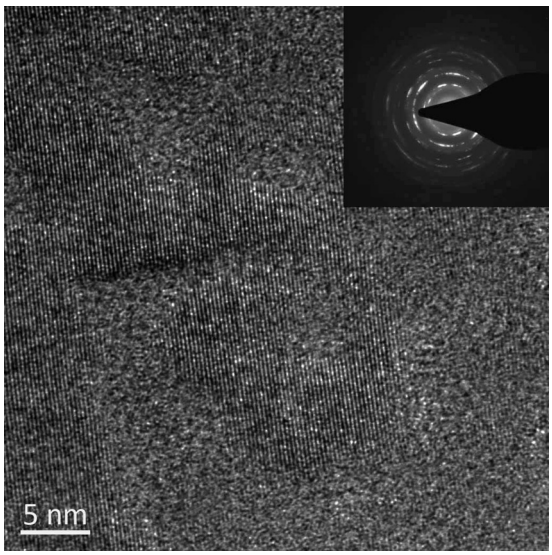

FIG. 4. Bright-field micrograph and associated diffraction pattern of the sample in Fig. 3 after aging it at room temperature for a week (see text). Note the increase in diffuse scattering relative to the fresh film. However, the preferred orientation, extending across the grain boundary, is still intact.

The diffraction pattern of the aged film shown in Fig. 4 exhibited an increase in the diffuse scattering (compare Fig. 4 with Fig. 3) suggestive of an increased disorder. This is possibly due to enhanced surface scattering or the creation of a disordered dead layer by oxidation process at the film-air boundary. Energy-dispersive spectroscopy revealed a 10–15% increase in oxygen content in the aged film relative to the fresh sample without a noticeable change in the Ge/Te ratio (being $\approx 0.9 \pm 0.05$). X-ray photoelectron spectroscopy on GeTe pellets exposed to laboratory atmosphere found adventitious layers of carbon on their surface, which may also be a source of enhanced scattering in films exposed to air. Another difference is the relative intensity of some rings that became more noticeable in the aged sample. Selected-area diffraction, sampling a circle of 0.8 μm diameter, was used to scan across the sample and the same features were observed throughout, so structural inhomogeneities in this material are probably limited to spatial scales $\leqslant 1$ μm.

The Hall effect that was monitored for some of the films showed a rather small change during the aging process; for a ≈100% increase of the film $R_\square$, the Hall resistance increased by ≈6%. Based on these Hall-effect measurements, the carrier concentration n of the films was $N = (1.5\text{–}2) \times 10^{20}$ cm^{-3}, somewhat smaller than the $N = (4\text{–}9) \times 10^{20}$ cm^{-3} found in the $GeSb_xTe_y$ compound [13]. In both cases, the Hall effect had the sign of a p-type carrier, consistent with theoretical prediction for the material [18]. The latter, based on equilibrium concentration of Ge vacancies in the ideal crystal, anticipated carrier concentration of $\approx 10^{19}$ cm^{-3} holes. The carrier concentration in our films, larger by roughly one order of magnitude, is probably a result of the abundant structural defects (readily observable in the TEM micrographs of Figs. 3 and 4) that apparently allow more Ge vacancies than the ordered crystal can sustain in equilibrium.

B. Measurement techniques

Conductivity of the samples was measured using a two-terminal ac technique employing a 1211-ITHACO current preamplifier and a PAR-124A lock-in amplifier. All measurements were performed with the samples immersed in liquid helium at $T \approx 4.1$ K held by a 100 liter storage dewar. This allowed up to two months of measurements on a given sample while keeping it cold (and in the dark), which was utilized to extend the time duration of the relaxation processes as well as many cycles of excitation-relaxation experiments. Fuller measurement techniques related to electron-glass properties are described elsewhere [19].

The ac voltage bias in conductivity measurements was small enough to ensure near-ohmic conditions (except for the current-voltage plots and the "stress protocol" described in Sec. II). Optical excitations in this work were accomplished by exposing the sample to an AlGaAs diode operating at $\approx 0.88 \pm 0.05$ μm, mounted on the sample stage typically ≈10–15 mm from the sample. The diode was energized by a computer-controlled current source (Keithley 220).

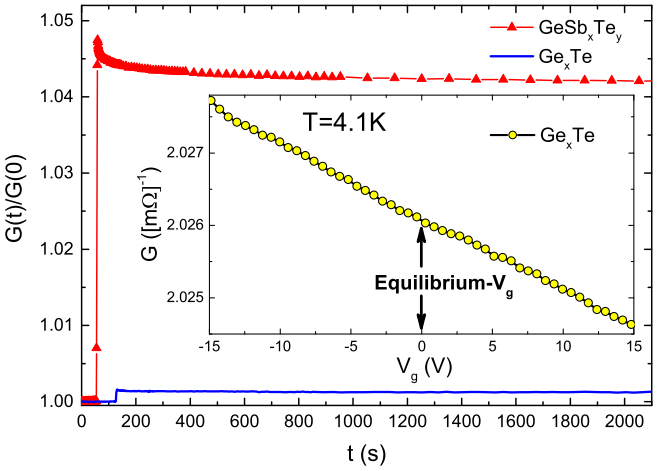

FIG. 5. Comparing the persistent-photoconductivity effect typically observed in our Ge_xTe samples with that of a $GeSb_xTe_y$ film. The $R_\square$ of the Ge_xTe film used here is 5 kΩ, while the $R_\square$ of the $GeSb_xTe_y$ film is 3 kΩ. The same protocol was used for both samples: same infrared intensity, distance from film, and duration of exposure. Inset shows the field effect for the Ge_xTe film.

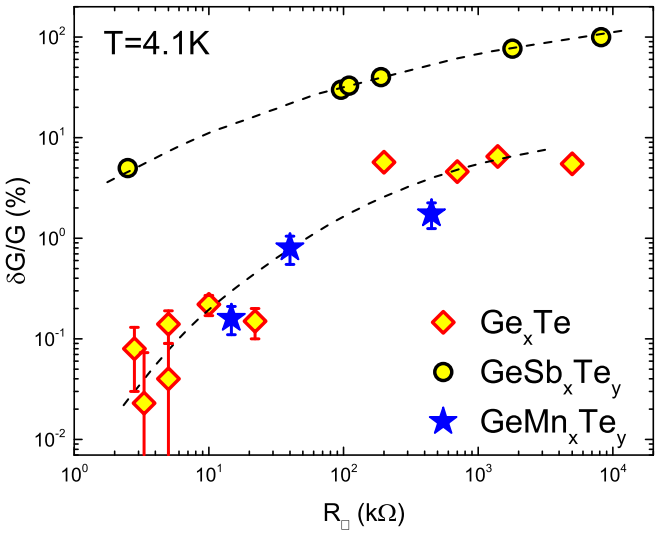

FIG. 6. The relative magnitude of the infrared-induced excess conductance in the PPC state for our Ge_xTe films as a function of their $R_\square$. These data are compared with the respective data for the $GeSb_xTe_y$ studied previously [13] and measured under the same conditions. Also shown are results for three Mn-doped Ge_xTe samples. Dashed lines are guides to the eye.

II. RESULTS AND DISCUSSION

A. Persistent photoconductivity in Ge_xTe

A main difference between the transport properties of Ge_xTe and the $GeSb_xTe_y$ alloy is their different sensitivity to optical excitation. The experimental protocol used for observing photoconductivity is illustrated in Fig. 5 using a diffusive Ge_xTe film with $R_\square = 5$ kΩ and, for comparison, a $GeSb_xTe_y$ film with similar $R_\square$ and thickness measured under the same conditions. The experiment begins ≈24 hours after the sample is cooled down to 4.1 K by recording $G(t)$ for 1–2 minutes to establish a baseline conductance G_0. The IR source is then turned on for 3 seconds, then turned off while $G(t)$ continues to be measured. The brief IR burst causes G to promptly increase by δG_{IR}, which decays slowly with time once the source is turned off (Fig. 5). Both samples exhibit excess conductance that persists for a long time after the optical excitation. In terms of magnitude, the persistent photoconductivity (PPC) signal is, however, much more conspicuous in the $GeSb_xTe_y$ film at all values of $R_\square$. A detailed comparison of the PPC magnitude versus $R_\square$ illustrating the difference between the two systems is given in Fig. 6. This figure includes three $GeMn_xTe_y$ samples. These were prepared by codepositing Mn with the Ge_xTe compound to test the effect of magnetic impurities. The Mn inclusion had only a small effect on the samples mobility, reducing it by 10–20% (for ≈20% Mn) relative to the pure compound. As shown in Fig. 6, it also had a negligible effect on the PPC performance of the compound.

Actually it appears that the PPC in pure Ge_xTe and the $GeMn_xTe_y$ compound differs from that in the $GeSb_xTe_y$ system not just by magnitude. The relaxation law that fits the time dependence of the excess conductance δG_{IR} in the $GeSb_xTe_y$ compounds showed a rather good fit to a stretched exponential law: $\delta G_{IR}(t) \propto \exp\{-(t/\tau)^\beta\}$ with $\beta = 0.1$ for all samples with $R_\square$ in the 10^3–10^7 Ω range. A similar expression could be fitted to the PPC data of our most resistive Ge_xTe films (δG_{IR} for the lower resistance samples was too small to allow a meaningful fit) but with $\beta = 0.14$–0.22. An example of a fit is shown in Fig. 7.

This, and the much smaller δG_{IR} (all other things being equal), suggest that the presence of the Sb plays a similar role in enhancing the PPC performance in germanium-telluride compounds as that of In impurities in lead-telluride alloys [20]. It would be of interest to find what other elements are effective in enhancing PPC in these systems. That is important for understanding the basics of the PPC phenomenon, but also as a tool for elucidating the physics of the electron glass; the PPC, when prominent enough, may be an effective way to increase the carrier concentration in a system, which is an

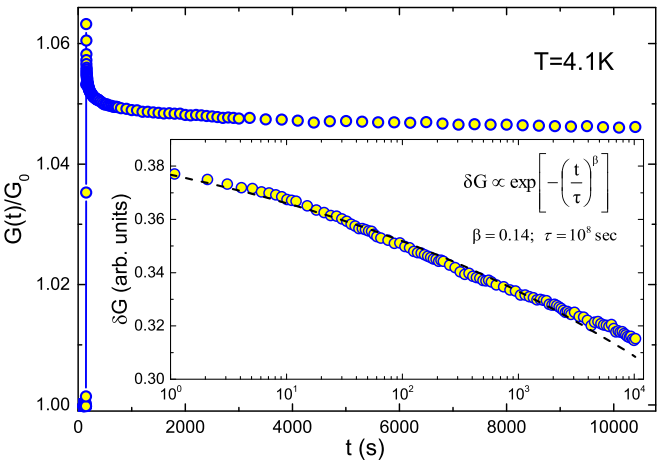

FIG. 7. The persistent photoconductivity of a Ge_xTe film with $R_\square = 750$ kΩ. The inset depicts a fit (dashed line) to a stretched exponent for the associated excess conductance as a function of time.

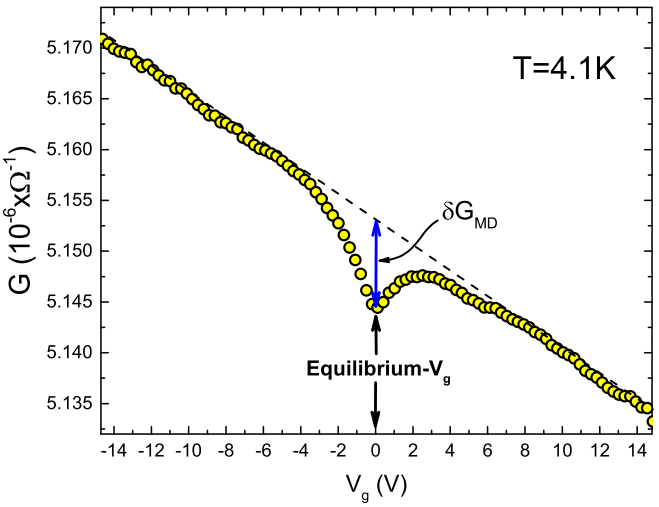

FIG. 8. The field effect for a Ge_xTe sample with $R_\square = 195$ kΩ showing a memory dip with a relative magnitude of ≈0.75% magnitude (defined by $\delta G_{MD}/G_{eq}$, where G_{eq} is the equilibrium value of the conductance at the bath temperature). The dashed line is the thermodynamic part of the field-effect measurement (as in the weakly disordered sample in Fig. 5).

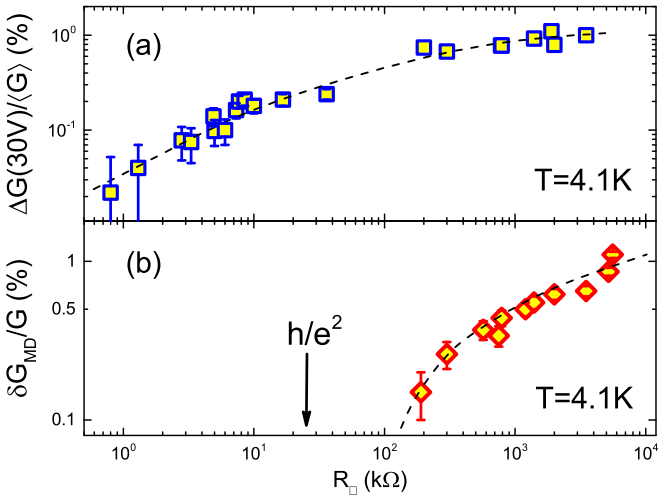

FIG. 9. (a) The relative change of conductance of the antisymmetric part of the field effect as a function of the Ge_xTe films $R_\square$. It is defined as $G(-30V)/G(+30V) - 1$. (b) The relative magnitude of the memory dip for the GeTe films as a function of their $R_\square$. Dashed lines are guides to the eye.

important parameter in controlling the dynamics of the electron glass [21].

B. Strongly localized Ge_xTe is an intrinsic electron glass

Like in previously studied materials, a prerequisite for observing electron-glass features is that the system must be strongly localized. This applies in particular to the appearance of a memory dip (MD) in the field-effect measurement, which is the identifying signature of the intrinsic [13] electron glass. A memory dip appeared in our films at $T \approx 4$ K once their $R_\square \gg \hbar/e^2$. A well-developed MD can be seen in Fig. 8 for a Ge_xTe film with $R_\square = 195$ kΩ.

The sign of $\frac{\partial}{\partial V_g}G(V_g)$ (reflecting how thermodynamic density of states $\partial n/\partial\mu$ changes with energy) is consistent with hole conduction (Figs. 2 and 8) and the sign of Hall-effect measurements on these films. Both the slope of $G(V_g)$ and the relative magnitude of the MD increases with disorder, as shown in Fig. 9. The disappearance of the MD as the system approaches the diffusive regime is common to *all* intrinsic electron glasses, and has been seen in both two-dimensional and three-dimensional systems [22]. This is a crucial attribute of the phenomenon and should be the starting point for any theoretical model.

As may be expected, Ge_xTe films that exhibit MD also show the other characteristic features of electron glasses. Figure 10 shows the excitation and ensuing relaxation of the excess conductance due to a sudden change of the gate voltage.

Another way to take the system away from equilibrium is the "stress protocol" [23]. By applying sufficiently strong electric field across the sample (between the "source" and "drain"), the system accumulates energy in excess of its thermal energy. This translates into excess conductance ΔG building up over the time the field is on. Once the strong field is removed and the conductance is monitored under ohmic conditions, ΔG decays with time and G approaches its equilibrium value. Both the buildup and decay of ΔG involve a protracted process. Unlike the sudden increase of G when V_g is switched (Fig. 10), ΔG grows continuously throughout the stress period without saturating. This is the analog of the "time-dependent heat capacity" typical of glasses [24], which is due to the wide temporal spectrum of the system degrees of freedom. The stress protocol is illustrated in Figs. 11(a) and 11(b) for the conductance evolution $G(t)$ during the relaxation and during the stress, respectively. The conductance dependence on the applied voltage of this sample is shown in

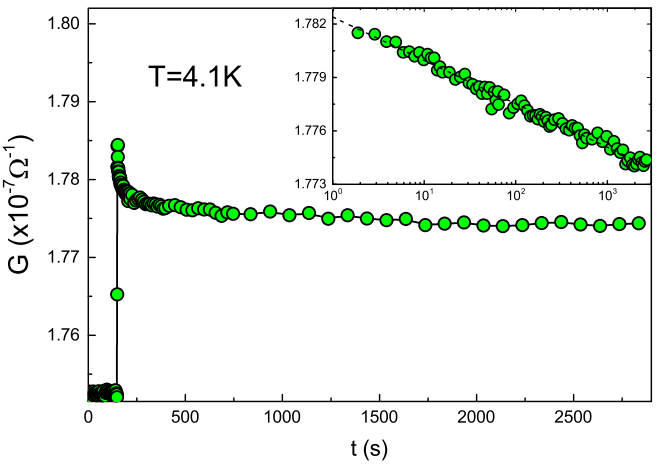

FIG. 10. Conductance vs time describing excitation of the electron glass by a sudden change of the gate voltage. Sample has $R_\square = 5.6$ MΩ. The protocol involved a fast sweep of V_g (within 2 s) from the equilibrium value $V_g = 0$ V, where the system spent 24 hours, to $V_g = -10$ V, where it was left for the duration of the time shown. The inset illustrates the logarithmic relaxation law of the excess conductance produced by the V_g change.

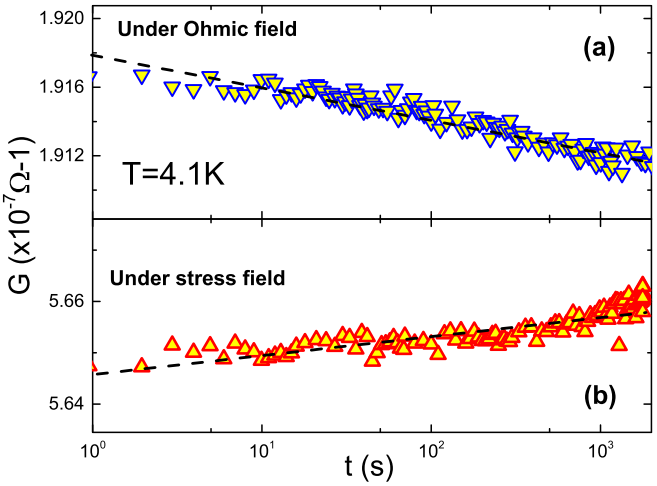

FIG. 11. The two parts of the stress protocol used on a Ge_xTe sample with $R_\square = 5.4\,M\Omega$. (a) Relaxation of the excess conductance after the stress was relieved. (b) The slow conductance buildup during the time stress was on.

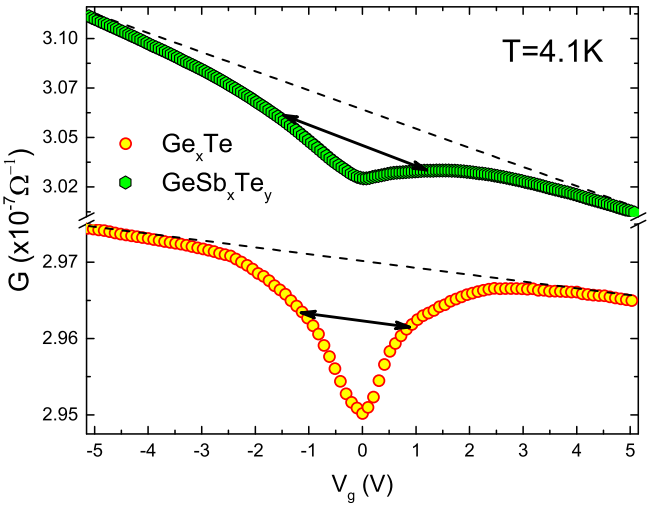

FIG. 13. Comparing the memory dip of a Ge_xTe sample with $R_\square = 3\,M\Omega$ with the memory dip of a $GeSb_xTe_y$ sample with $R_\square = 6.2\,M\Omega$. Both $G(V_g)$ curves were taken with the same sweep rate. The arrows delineate the typical width of each memory dip.

Fig. 12 with the voltage values used during the stress and relaxation periods marked on the $G(V)$ curve.

The results of the stress protocol (Fig. 11) are essentially the same in all previously studied systems that exhibit electron-glass attributes [25]. Qualitatively different behavior has been observed in granular systems [26]. Granular systems differ from Anderson insulators in other aspects as well, although they share some glassy features such as a memory dip [27].

It is also worth commenting on the mechanism by which the applied nonohmic field takes the system out of equilibrium. The enhanced conductance that appears immediately after applying the field is associated with adiabatic modification of the hopping probabilities [28]. This is the dominant effect when the resistance is large, but Joule heating is to some degree also responsible for the increase of G when a large voltage is applied (except when the applied field frequency exceeds the

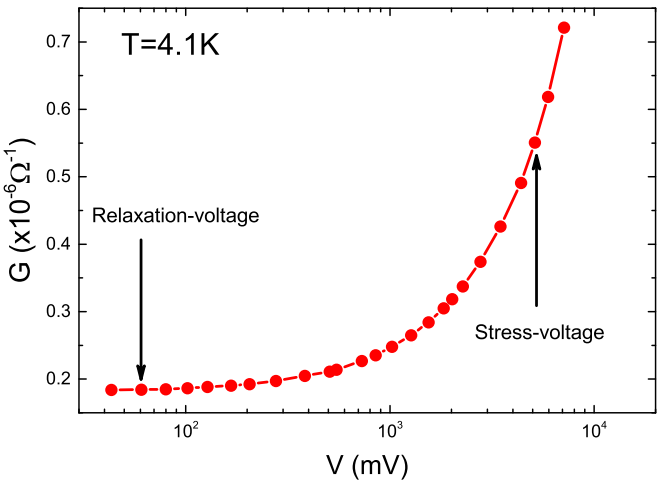

FIG. 12. The conductance of the sample used for the stress protocol (Fig. 11) as a function of the applied voltage. Sample dimensions are $L = W = 0.5$ mm. Marked by arrows are the voltages used during the stress and relaxation periods.

electron-phonon inelastic rate [29]). Joule heating is the reason for the slow buildup of excess conductance observed under large voltages. Qualitatively similar behavior is achieved by raising the bath temperature. However, comparing the behavior of $G(t)$ under field F versus that of raising the bath temperature by ΔT (to achieve the same initial ΔG) demonstrated that under ΔT, the ensuing excess conductance increased with time at a faster rate [30]. This is just a manifestation of the fact alluded to above: heating is only part of the reason for nonohmicity in the hopping regime. The advantage of using voltage swings over raising/lowering the bath temperature is the higher speed and controllability of the procedure. The price is the uncertainty in assigning a value of "effective temperature" to the stress protocol: the value of G under nonohmic fields is, in general, not a reliable thermometer; nonohmic measurements of $G(V)$ are *not* simply related to the *equilibrium* values of $G(T)$.

As mentioned above, the visibility of the memory dip, over the antisymmetric $G(V_g)$ [controlled by the energy dependence of the thermodynamic density of states (DOS)], increases with $R_\square$. The memory dip for one of the most resistive samples we were able to manufacture in this study is shown in Fig. 13, where it is compared with the MD of a $GeSb_xTe_y$ film with the same $R_\square$ and measured under the same conditions (temperature, sweep rate, and gate-voltage range).

The main difference between the two $G(V_g)$ curves in Fig. 13 is the steeper antisymmetric contribution of the $GeSb_xTe_y$ sample. Closer examination reveals that the typical width of the MD is also somewhat wider for the Sb-doped alloy. The narrower width of the MD in Ge_xTe may be a result of the smaller carrier concentration in this material, which is in line with the general trend observed in previously studied electron glasses. To date, however, the only material where it was possible to change the carrier concentration over a considerable range is amorphous indium-oxide [15]. The carrier concentration in Ge_xTe is associated with Ge vacancies [17] and, as demonstrated by Bahl and Chopra, the

carrier concentration in this system can be varied over a decade by heat treatment during crystallization [16]. Ge_xTe may then be another system that allows testing the relation between the carrier concentration, glass dynamics, and the MD width by either controlling the sample stoichiometry during deposition, alloying with foreign elements, or thermal annealing. Future work will also focus on modifying the transport parameters of this system by various dopants.

With the addition of the currently studied Ge_xTe, there are now seven different Anderson-localized systems that exhibit intrinsic electron-glass effects. The previously studied systems and their properties were discussed elsewhere [25]. The only feature common to all of these systems is having relatively large carrier concentration: $N \geqslant 5 \times 10^{19}$ cm^{-3}. These systems have quite different structural properties, making it hard to conceive of a common defect that might be responsible for the long relaxation times observed in their nonequilibrium transport properties. Grain boundaries, for example, are not likely to be relevant as their contribution to transport must be very weak in Ge_xTe relative to other electron glasses, while the electron-glass effects exhibited by all of these systems are very similar: they all show slow relaxation and a memory dip. It is therefore more likely that it is the *magnitude* of the disorder rather than its specific nature that is the important factor. This, in turn, suggests that quantifying the disorder in the Anderson-insulating phase may be a vital step in the quest to unravel the mechanism responsible for the electron-glass dynamics.

ACKNOWLEDGMENTS

This research has been supported by Grant No. 1126/12 administered by the Israel Academy for Sciences and Humanities.

[1] N. F. Mott, Philos. Mag. **26**, 1015 (1972).
[2] J. H. Davies, P. A. Lee, and T. M. Rice, Phys. Rev. Lett. **49**, 758 (1982); M. Grünewald, B. Pohlman, L. Schweitzer, and D. Würtz, J. Phys. C **15**, L1153 (1982); J. H. Davies, P. A. Lee, and T. M. Rice, Phys. Rev. B **29**, 4260 (1984).
[3] M. Pollak and M. Ortuño, Sol. Energy Mater. **8**, 81 (1982); M. Pollak, Philos. Mag. B **50**, 265 (1984).
[4] G. Vignale, Phys. Rev. B **36**, 8192 (1987).
[5] C. C. Yu, Phys. Rev. Lett. **82**, 4074 (1999).
[6] M. Müller and L. B. Ioffe, Phys. Rev. Lett. **93**, 256403 (2004).
[7] V. Malik and D. Kumar, Phys. Rev. B **69**, 153103 (2004).
[8] R. Grempel, Europhys. Lett. **66**, 854 (2004).
[9] E. Lebanon and M. Müller, Phys. Rev. B **72**, 174202 (2005); M. Müller and E. Lebanon, J. Phys. IV France **131**, 167 (2005).
[10] A. Amir, Y. Oreg, and Y. Imry, Phys. Rev. B **77**, 165207 (2008); Annu. Rev. Condens. Matter Phys. **2**, 235 (2011); Y. Meroz, Y. Oreg, and Y. Imry, Europhys. Lett. **105**, 37010 (2014).
[11] M. Pollak, M. Ortuño, and A. Frydman, *The Electron Glass* (Cambridge University Press, Cambridge, 2013).
[12] M. Ben-Chorin, D. Kowal, and Z. Ovadyahu, Phys. Rev. B **44**, 3420 (1991); M. Ben-Chorin, Z. Ovadyahu, and M. Pollak, *ibid.* **48**, 15025 (1993).
[13] Z. Ovadyahu, Phys. Rev. B **91**, 094204 (2015).
[14] Z. Ovadyahu, Phys. Rev. B **78**, 195120 (2008).
[15] A. Vaknin, Z. Ovadyahu, and M. Pollak, Phys. Rev. Lett. **81**, 669 (1998).
[16] S. K. Bahl and K. L. Chopra, J. Appl. Phys. **41**, 2196 (1970). More recent work was done on alloys based on this material mostly for study of the so-called *phase-change materials*; for a review, see S. Raoux, Annu. Rev. Mater. Res. **39**, 25 (2009), and for a study of the metal-insulator transition in these compounds, see T. Siegrist, P. Jost, H. Volker, M. Woda, P. Merkelbach, C. Schlockermann, and M. Wuttig, Nat. Mater. **10**, 202 (2011).
[17] M. G. Craford, G. E. Stillman, J. A. Rossi, and N. Holonyak, Phys. Rev. **168**, 867 (1968); D. V. Lang and R. A. Logan, Phys. Rev. Lett. **39**, 635 (1977); D. V. Lang, R. A. Logan, and M. Jaros, Phys. Rev. B **19**, 1015 (1979); H. J. Queisser and D. E. Theodorou, Phys. Rev. Lett. **43**, 401 (1979); J. Misuraca, J. Trbovic, J. Lu, J. Zhao, Y. Ohno, H. Ohno, P. Xiong, and S. von Molnár, Phys. Rev. B **82**, 125202 (2010).
[18] A. H. Edwards, A. C. Pineda, P. A. Schultz, M. G. Martin, A. P. Thompson, and H. P. Hjalmarson, J. Phys.: Condens. Matter **17**, L329 (2005); A. H. Edwards, A. C. Pineda, P. A. Schultz, M. G. Martin, A. P. Thompson, H. P. Hjalmarson, and C. J. Umrigar, Phys. Rev. B **73**, 045210 (2006).
[19] A. Vaknin, Z. Ovadyahu, and M. Pollak, Phys. Rev. B **65**, 134208 (2002).
[20] B. A. Akimova, V. Dmitriev, R. Khokhlov, and L. I. Ryabova, Phys. Stat. Sol. A **137**, 9 (1993).
[21] Z. Ovadyahu, Phys. Rev. Lett. **115**, 046601 (2015).
[22] Z. Ovadyahu, Phys. Rev. B **90**, 054204 (2014).
[23] V. Orlyanchik and Z. Ovadyahu, Phys. Rev. Lett. **92**, 066801 (2004).
[24] S. M. Wolpert, A. Weitz, and B. Wunderlich, J. Polym. Sci. **9**, 1887 (1971).
[25] Z. Ovadyahu, Phys. Rev. B **88**, 085106 (2013).
[26] N. Kurzweil and A. Frydman, Phys. Rev. B **75**, 020202 (2007).
[27] C. J. Adkins, J. D. Benjamin, J. M. D. Thomas, J. W. Gardner, and A. J. McGeown, J. Phys. C: Solid State Phys. **17**, 4633 (1984); G. Martinez-Arizala, D. E. Grupp, C. Christiansen, A. M. Mack, N. Markovic, Y. Seguchi, and A. M. Goldman, Phys. Rev. Lett. **78**, 1130 (1997); G. Martinez-Arizala, C. Christiansen, D. E. Grupp, N. Marković, A. M. Mack, and A. M. Goldman, Phys. Rev. B **57**, R670(R) (1998); T. Grenet, Eur. Phys. J. **32**, 275 (2003); T. Grenet, J. Delahaye, M. Sabra, and F. Gay, Eur. Phys. J. B **56**, 183 (2007); T. Havdala, A. Eisenbach, and A. Frydman, Europhys. Lett. **98**, 67006 (2012).
[28] R. M. Hill, Philos. Mag. **24**, 1307 (1971); B. I. Shklovskii, Fiz. Tekh. Poluprovodn. **6**, 2335 (1972); Sov. Phys. Semicond. **6**, 1964 (1973); N. Apsley and H. P. Hughes, Philos. Mag. **31**, 1327 (1975); M. Pollak and I. Riess, J. Phys. C **9**, 2339 (1976).
[29] Z. Ovadyahu, Phys. Rev. Lett. **108**, 156602 (2012).
[30] Z. Ovadyahu, Phys. Rev. B **73**, 214208 (2006).